This article has been accepted for inclusion in a future issue of this journal. Content is final as presented, with the exception of pagination.

Performance Evaluation of Novel Strain-Engineered Ge-InGaAs Heterojunction Tunnel Field-Effect Transistors

Jheng-Sin Liu, *Student Member, IEEE*, Michael B. Clavel, *Student Member, IEEE*, and Mantu K. Hudait, *Senior Member, IEEE*

***Abstract*— Novel strain-engineered staggered gap Ge/In_xGa_{1-x}As heterojunction tunnel FETs (H-TFETs) are proposed and theoretically evaluated. Modulation of the indium alloy composition at the source–channel heterointerface resulted in 18.6× and 16.9× enhancement in I_{ON} for n- and p-channel Ge/In_xGa_{1-x}As H-TFETs, respectively, as compared with strained Ge homojunction TFETs (p^+-Ge/i-Ge/n^+-Ge). The n-type H-TFETs (p^+-Ge/i-In_xGa_{1-x}As/n^+-In_xGa_{1-x}As) exhibited superior leakage suppression due to a larger tunneling barrier at the channel–drain interface. Moreover, the p-type H-TFETs (n^+-In_xGa_{1-x}As/i-Ge/p^+-Ge) demonstrated a significant enhancement in I_{ON} due to an unequal shift in the conduction band edge as a result of doping-induced bandgap narrowing. The simulated tensile-strained Ge/In_xGa_{1-x}As H-TFETs show a great promise for ultralow-power switches with high ON-state and low OFF-state current, providing a new path for low-power complimentary TFET logic.**

***Index Terms*— Ge/InGaAs heterojunctions, InGaAs, strained Ge, tunnel FETs (TFETs).**

I. INTRODUCTION

THE aggressive scaling of silicon (Si)-based nanoscale transistor technology has led to an unprecedented performance enhancement, while facing several technical challenges to reduce the active power dissipation and OFF-state leakage current. Tunnel FETs (TFETs), operating in the band-to-band tunneling (BTBT) mechanism, are being investigated as a potential candidate to obtain steep subthreshold swing (SS) characteristics, and thereby greatly reducing the static power consumption through low supply voltage device operation. Recently, narrow bandgap materials, such as group III–V [1], [2] and germanium (Ge) [3]–[5], have been comprehensively studied for high-performance TFET applications. Heterojunction TFETs (H-TFETs) fabricated from Ge on GaAs [6] and relaxed Ge on $In_{0.53}Ga_{0.47}$As [7] have also been demonstrated. Of particular interest for the future H-TFET architectures, biaxial tensile-strained Ge (ε-Ge) epitaxially grown on III–V template [8] provides a method for achieving high ON-state current (I_{ON}) through the conversion of Ge from an indirect-to-direct bandgap semiconductor, and thus resulting in an enhanced tunneling probability.

Recently, we have demonstrated the integration of device quality ε-Ge on In_xGa_{1-x}As virtual substrates by separate solid source molecular beam epitaxy chambers for III–V and Ge, connected through an ultrahigh vacuum transfer chamber [8]. In this paper, we have investigated the role of strain and indium (In) alloy composition on the device performance of Ge homojunction (homo-TFETs, p^+-Ge/i-Ge/n^+-Ge) and Ge/In_xGa_{1-x}As H-TFETs in Γ–Γ BTBT (strain > 1.5%). Using computer-aided design software (TCAD Sentaurus), we demonstrate a significant strain-dependent enhancement in I_{ON} current for both n- and p-type Ge H-TFETs. Moreover, we show that a combination of strain and strain template In composition in In_xGa_{1-x}As result in the highest reduction of effective tunnel barrier height ($E_{b_{\mathrm{eff}}}$) for Ge-based H-TFET architectures, allowing for an increased tunneling probability, which further enhances in I_{ON} current and a decrease in SS.

II. DEVICE STRUCTURES AND PHYSICAL MODELS

A. Band Alignment and Quantum Confinement

Staggered gap band alignment is the core of ε-Ge/In_xGa_{1-x}As H-TFETs. The effect of the quantization and the heterojunction band alignment was included in our model. For ε-Ge/In_xGa_{1-x}As heterointerface, we employed 30 × 30 k · p model [9] to the energy band structure of in-plane biaxial tensile-strained Ge (001). Fig. 1 shows the calculated conduction and valence band shifts with in-plane biaxial tensile-strained Ge (001). With increased tensile strain, the lowest conduction energy in L- and Γ-valley crossed over at ∼1.5% strain, which is an excellent agreement with the previous reported value [10]. However, high tensile strain (>1.5%) will provide not only the smaller bandgap but also the direct bandgap in nature. The advantage for direct bandgap Ge was to enhance the tunneling probability by eliminating the phonon from the tunneling processes.

Manuscript received June 21, 2015; revised July 23, 2015 and August 10, 2015; accepted August 13, 2015. The work of J.-S. Liu and M. B. Clavel was supported by the Division of Electrical, Communications and Cyber Systems through the National Science Foundation under Grant ECCS-1348653. The review of this paper was arranged by Editor G. Ghione.

The authors are with the Department of Electrical and Computer Engineering, Virginia Polytechnic Institute and State University, Blacksburg, VA 24061 USA (e-mail: jsliu@vt.edu; mbclavel@vt.edu; mantu@vt.edu).

Color versions of one or more of the figures in this paper are available online at http://ieeexplore.ieee.org.

Digital Object Identifier 10.1109/TED.2015.2469536

0018-9383 © 2015 IEEE. Personal use is permitted, but republication/redistribution requires IEEE permission.
See http://www.ieee.org/publications_standards/publications/rights/index.html for more information.

This article has been accepted for inclusion in a future issue of this journal. Content is final as presented, with the exception of pagination.

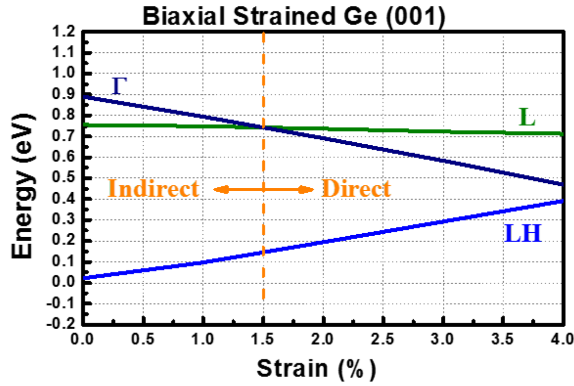

Fig. 1. Calculated conduction and valence band shifts with in-plane biaxial tensile-strained applied to Ge (001). The bandgap of Ge converts from indirect-to-direct bandgap with 1.5% biaxial tensile strain.

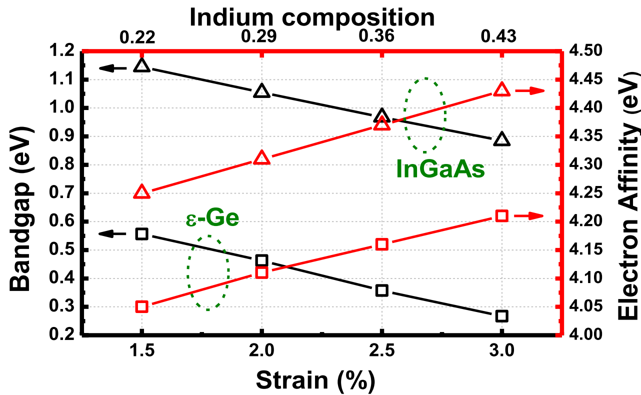

Fig. 2. Calculated direct bandgaps (black lines) and electron affinity (red lines) for Ge (squares) and InGaAs (triangles).

On the other hand, $In_xGa_{1-x}As$ material is a direct bandgap material system for any composition of In. As a result, this heterojunction system can provide Γ–Γ BTBT from ε-Ge to $In_xGa_{1-x}As$, which was originally L–Γ BTBT process in the Ge homojunction system. In this paper, we have considered the highly tensile-strained systems (>1.5%) in our model. We have also used the bandgap relation $E_g = 1.456 - 1.5x + 0.4x^2$ as a function of gallium alloy composition in InGaAs, and the electron affinity was estimated using Vegard's law, $\chi_{In_xGa_{1-x}As} = x \cdot \chi_{InAs} + (1-x) \cdot \chi_{GaAs}$ [11]. Fig. 2 shows the calculated direct bandgaps of Ge and InGaAs, and electron affinity for both materials as a function of strain.

To simulate improved channel control, a long-channel, double-gated TFET configuration was utilized in conjunction with a low effective oxide thickness. Both conduction and valence band edge shifted due to the quantum confinement effect in this structure. The influence of quantum confinement effects, shown in Fig. 3(a) using Nextnano3, on device performance, was considered [12]. This Nextnano3 simulator solves Schrödinger–Poisson equation in 1-D with SiO_2/Ge/SiO_2 structure for 1.5% strain, and a device band diagram along a 1-D cut perpendicular to gate electrode is shown in Fig. 3(a) (inset). The new ground state energies created by quantization effect are located below and above the original band edges (shown in orange line and pink line), where ΔE_c and ΔE_v are the conduction and the

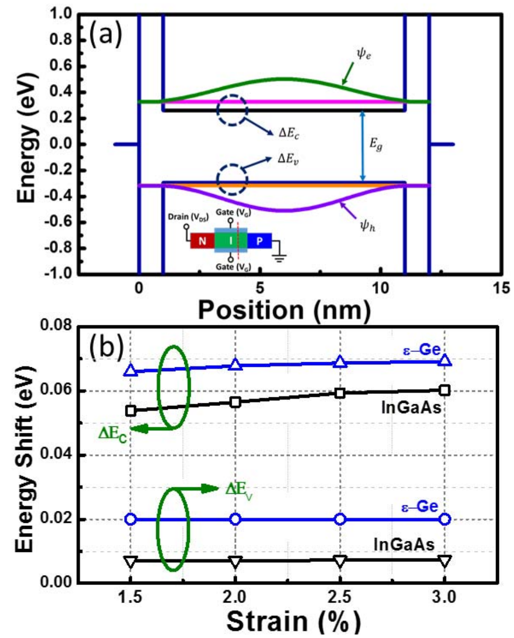

Fig. 3. (a) Band diagram of SiO_2/Ge/SiO_2 (1/10/1 nm) for quantum confinement simulation. (b) Valance band shift, ΔE_v and conduction shift, ΔE_c as a function of strain in Ge and InGaAs channel.

valence band shift, respectively. These energy shifts due to quantization effect further changed the effective bandgap, electron affinity, and band alignments. For strained Ge, the effective mass also changed with different amounts of strain. Moreover, with increasing strain, ΔE_c and ΔE_v are also increased further [shown in Fig. 3(b)] due to the decrease in out-of-plane [001] electron effective mass ($m_{c,\text{op}}$). The change in out-of-plane [001] effective mass as a function of strain amount used in simulation was extracted from [13] and also listed in Table I.

Utilizing two main mechanisms (i.e., quantization and strain effect) for band alignment calculation, the schematics of p-type and n-type strain-engineered Ge/$In_xGa_{1-x}As$ H-TFETs studied in this paper are shown in Fig. 4(a) and (b), respectively. The bandgap narrowing (BGN) effect was also considered in source/drain regions of these tunnel FET structures. Therefore, the final values of electron affinity as well as bandgaps of Ge and InGaAs used in this paper are also listed in Table I. Fig. 4 shows the simulated band diagrams of the strain-engineered Ge/$In_xGa_{1-x}As$ H-TFETs studied in this paper including a p-type n^+-$In_xGa_{1-x}As$/i-Ge/p^+-Ge H-TFET [Fig. 4(a)] and an n-type p^+-Ge/i-$In_xGa_{1-x}As$/n^+-$In_xGa_{1-x}As$ H-TFET [Fig. 4(b)]. The selection in channel material for each device efficiently leverages the increased carrier mobilities of both materials (i-$In_xGa_{1-x}As$ for n-type and i-Ge for p-type structures). One can find from Fig. 4, the band diagrams exhibited a staggered (or type-II) band alignment, and thereby assisting in reduction of $E_{b_{\text{eff}}}$ and increase in tunneling probability. Moreover, the presence of high-strain (≥1.5%) within the ε-Ge layer is expected to convert the Ge to a direct-gap semiconductor [13], further enhancing the Γ–Γ tunneling probability from ε-Ge to $In_xGa_{1-x}As$.

This article has been accepted for inclusion in a future issue of this journal. Content is final as presented, with the exception of pagination.

TABLE I
SIMULATION PARAMETERS

Parameter Description	Value Used	Parameter Description	Value Used
Gate Length (L_g)	40 [nm]	Channel Length (L_c)	40 [nm]
Body Thickness (t_b)	10 [nm]	EOT	1 [nm]
Doping, $N_{source}=N_{drain}$	1×10^{19} [cm-3]	Source/Drain Length (L_s,L_D)	30 [nm]
A^1_{InGsAs}	0.0476 [eV]	C^1_{InGaAS}	0.0032 [eV]
A^2_{Ge}	8.15 [eV]	C^2_{Ge}	2.03 [eV]
Germanium Strain (%)	**m_{r_dir} (m_0)**	**A_{dir} ($cm^{-3}s^{-1}$)**	**B_{dir} (MV/cm)**
1.5	0.025	1.67e20	5.25
2.0	0.024	1.69e20	4.85
2.5	0.024	1.72e20	4.49
3.0	0.023	1.73e20	4.14
Germanium Strain (%)	**$m_{c,ip}$ (m_0)**	**$m_{c,op}$ (m_0)**	**$m_{v,op}$ (m_0)**
1.5	0.043	0.033	0.037
2.0	0.042	0.027	0.037
2.5	0.041	0.022	0.035
3.0	0.040	0.017	0.035
Germanium Strain (%), Indium Composition (%)	**Electron affinity (eV) (Ge, InGaAs)**	**Bandgap (eV) (Ge, InGaAs)**	
1.5, 22	4.05, 4.25	0.56, 1.15	
2.0, 29	4.11, 4.31	0.46, 1.06	
2.5, 36	4.16, 4.37	0.36, 0.97	
3.0, 43	4.21, 4.43	0.27, 0.89	

1. Pre-factors for the Jain-Roulston band gap narrowing model for n-type $In_xGa_{1-x}As$ [15].
2. Pre-factors for the Jain-Roulston band gap narrowing model for Γ-valley Ge [16].
3. Effective mass value, A_{dir} and B_{dir} are extracted from [13].

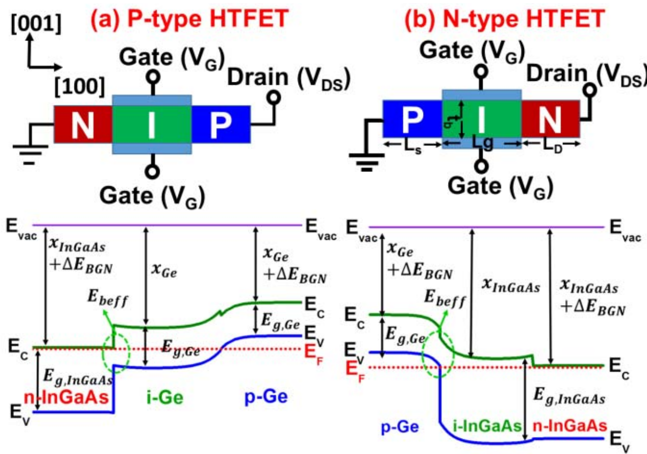

Fig. 4. Structural models and simulated schematic band diagrams used in the numerical device simulation of (a) p-type and (b) n-type heterojunction (ε-Ge/$In_xGa_{1-x}As$) TFETs.

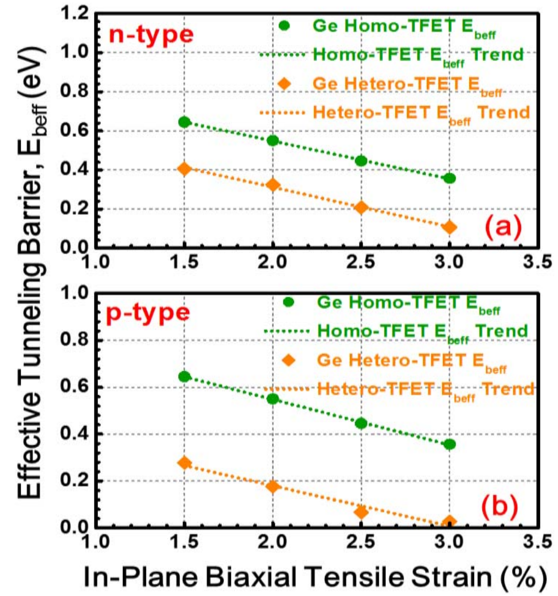

Fig. 5. Strain-induced reduction of the effective tunneling barrier height for (a) n-type and (b) p-type homojunction (ε-Ge) and heterojunction (ε-Ge/$In_xGa_{1-x}As$) TFETs.

B. Model and Parameters

For tensile-strained direct bandgap Ge, the direct BTBT model determining the generation rate per unit volume is expressed by [14]

$$G = A_{\text{dir}}(F)^P \exp\left(-\frac{B_{\text{dir}}}{F}\right) \quad (1)$$

where F (volt/centimeter) is the electric field and $P = 2$ is for the direct BTBT transition. Prefactors A_{dir} and B_{dir} are calculated from [13]. In the case of BGN, Jain–Roulston model was used and expressed as [15], [16]

$$\Delta E_{\text{BGN,InGaAs}} = A_{\text{InGaAs}}\left(\frac{N}{18}\right)^{1/3} + C_{\text{InGaAs}}\left(\frac{N}{18}\right)^{1/4} \quad (2)$$

$$\Delta E_{\text{BGN,Ge}} = A_{\text{Ge}}\left(\frac{N}{18}\right)^{1/4} + C_{\text{Ge}}\left(\frac{N}{18}\right)^{1/2} \quad (3)$$

where A and C are the prefactors.

This article has been accepted for inclusion in a future issue of this journal. Content is final as presented, with the exception of pagination.

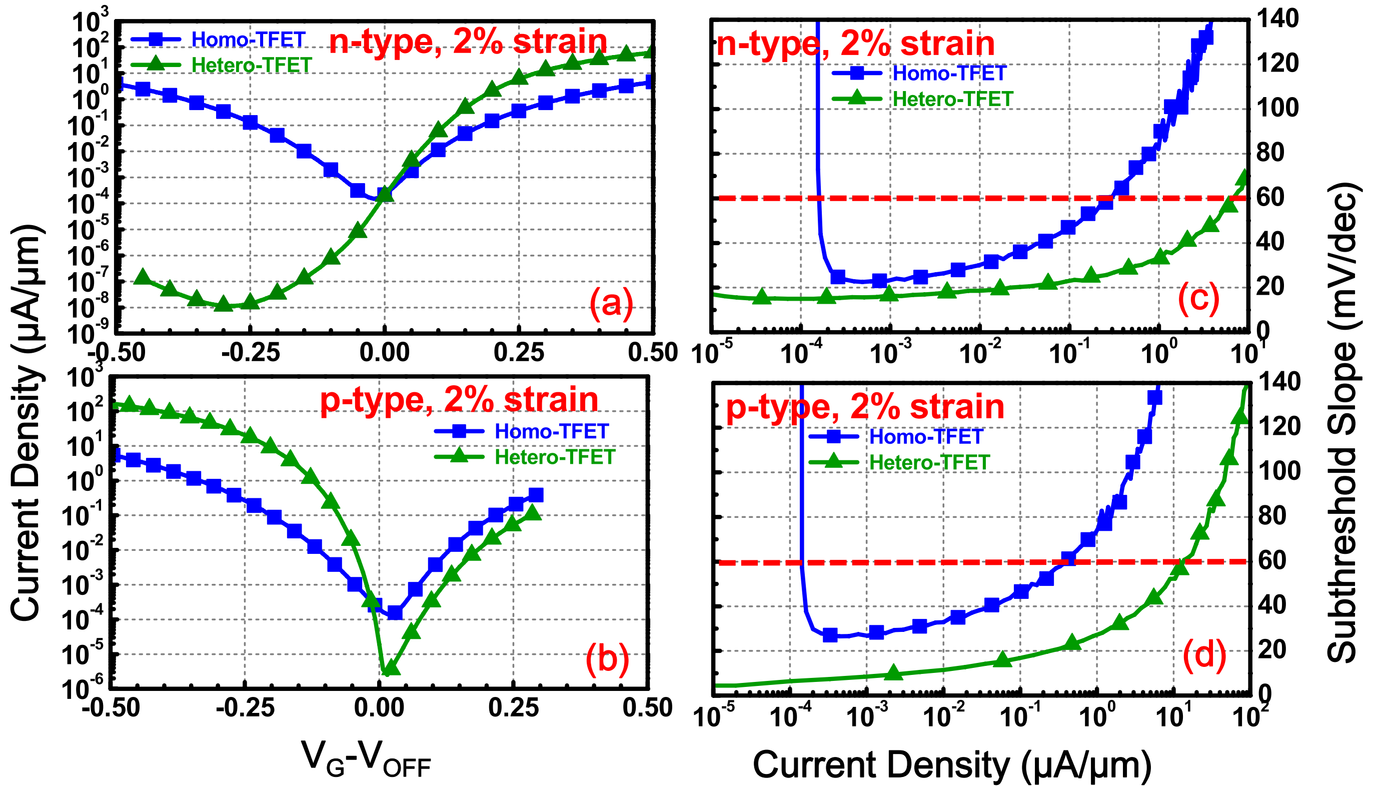

Fig. 6. Current–voltage and SS characteristics of (a) and (b) n-type and (c) and (d) p-type homojunction (ε-Ge) and heterojunction (ε-Ge/$In_xGa_{1-x}As$) TFETs.

In this paper, we have considered double-gated TFET structures with ultrathin body to gain the ability of gate control. The channel length (L_c) was equal to the gate length (L_g) of the device, and the channel was entirely covered by the gate. Symmetrically doped source and drain regions were utilized at first in our device simulation that helped us to understand the unipolar or ambipolar behavior of a TFET device structure. Synopsys' Sentaurus TCAD software [17] was used to simulate the double-gated p-i-n TFET structures using a Fermi–Dirac statistics model, a drift-diffusion carrier transport model, a doping-dependent mobility model [18], Auger and Shockley–Read–Hall generation/recombination models, a doping-dependent bandgap-narrow model, the strained density of state mass [19], and the dynamic nonlocal path BTBT model at 300 K. Table I summarizes all model parameters used in the TFET device simulation.

III. Result and Discussion

A. Effective Barrier Heights

The most important design parameter for a TFET device is the effective tunnel barrier height that controls the tunneling probability and hence the I_{ON} of the device. Thus, the effective barrier height ($E_{b_{\text{eff}}}$) can be expressed by: 1) $E_{b_{\text{eff}}} = (\chi_{\text{InGaAs}} + \Delta E_{\text{BGN,InGaAs}}) - (\chi_{\text{Ge}} + E_{g,\text{Ge}})$ for n-type and 2) $E_{b_{\text{eff}}} = (\chi_{\text{InGaAs}}) - (\chi_{\text{Ge}} + E_{g,\text{Ge}} + \Delta E_{\text{BGN,Ge}})$ for p-type, shown in Fig. 4, respectively. Fig. 5 shows $E_{b_{\text{eff}}}$ as a function of increasing biaxial tensile strain for n-type and p-type TFETs. Both ε-Ge-based TFET architectures benefited from strain-induced lowering of $E_{b_{\text{eff}}}$, however, H-TFETs experienced further reduction in $E_{b_{\text{eff}}}$ due to a larger intrinsic band discontinuity at the ε-Ge/$In_xGa_{1-x}As$ heterointerface [8]. This band discontinuity can be explained as a result of increasing In composition into the $In_xGa_{1-x}As$ layers translating into: 1) increased Ge strain; 2) a lowering of both ε-Ge and $In_xGa_{1-x}As$ bandgaps; and 3) a corresponding increase in the electron affinity of both materials. As a result, H-TFETs show superior modulation of $E_{b_{\text{eff}}}$ through strain engineering. Moreover, the p-type H-TFETs further benefited from doping-induced BGN in the n-$In_xGa_{1-x}As$ source. The unequal shift of the band edges in heavily doped $In_xGa_{1-x}As$ corresponds to a reduction in $E_{b_{\text{eff}}}$ in the p-type H-TFETs that is absent in n-type structures due to the intrinsic nature of the $In_xGa_{1-x}As$ at the source–channel heterojunction.

B. I–V Characteristics

Fig. 6(a) and (b) shows the simulated I_{DS}–V_{GS} characteristics as a function of overdrive voltage, V_{GS}–V_{OFF}, for the n-type and p-type homo- and H-TFETs under 2% biaxial strain, respectively. The OFF-state leakage current is matched at 200 pA/μm for all devices at V_{OFF} voltage. Both n- and p-type H-TFETs demonstrated superior I_{ON} over similarly strained homo-TFETs. The substantial enhancement in I_{ON} was attributed due to the smaller $E_{b_{\text{eff}}}$ at the source–channel heterointerface in both H-TFETs. Further enhancement can also be expected for the n-type H-TFETs due to the improved electron mobility in the i-$In_xGa_{1-x}As$ channel as compared with the strained i-Ge channel. $E_{b_{\text{eff}}}$ was found to be 0.55 eV for both homo-TFETs under 2% strain, whereas n- and p-type H-TFETs exhibited $E_{b_{\text{eff}}}$ of 0.32 and 0.18 eV, respectively, resulting in an enhanced tunneling probability.

This article has been accepted for inclusion in a future issue of this journal. Content is final as presented, with the exception of pagination.

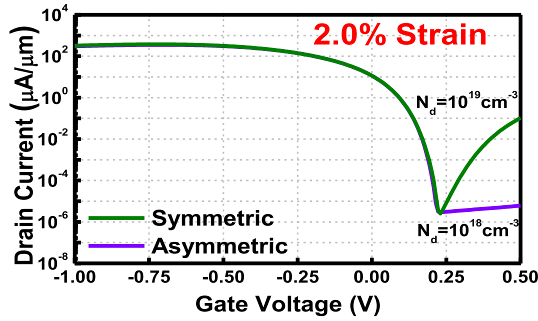

Fig. 7. Drain current as a function of gate voltage with two different drain doping concentrations.

Also shown in Fig. 6(c) and (d) are the SS characteristics for n- and p-type homo- and H-TFETs, respectively. The SS of both structures was below 60 mV/decade, which is the limitation of the conventional MOSFET devices. Moreover, the SS depends on the device structure and the channel passivation. Furthermore, the p-type H-TFETs exhibited enhanced SS reduction due to the lower $E_{b_{\text{eff}}}$, compared with n-type H-TFETs.

C. Ambipolar Behavior

The n-type H-TFETs exhibited significantly reduced OFF-state current (I_{OFF}) in comparison with both homo-TFETs and p-type H-TFETs. This reduction in I_{OFF} is due to the increased drain–channel tunneling barrier at the i-$\text{In}_x\text{Ga}_{1-x}\text{As}$/n$^+$-$\text{In}_x\text{Ga}_{1-x}\text{As}$ interface in the n-type TFETs (higher bandgap for $\text{In}_x\text{Ga}_{1-x}\text{As}$), and thereby suppressing the ambipolar behavior of the symmetrically doped devices. Conversely, the i-Ge/p$^+$-Ge channel–drain interface in the p-type H-TFETs mirrors the ε-Ge homo-TFET structure, and thus indicating that the dominate leakage mechanism in the p-type H-TFETs results from the ambipolar behavior of the device during the OFF-state. Moreover, though strain modulation reduces the ε-Ge bandgap and reduces $E_{b_{\text{eff}}}$ between the source and channel, it can be clearly seen from Fig. 6(a) and (b) that the lowering of $E_{b_{\text{eff}}}$ for ε-Ge-based homo-TFETs drastically reduced $I_{\text{ON}}/I_{\text{OFF}}$ ratio due to the ambipolar characteristic, as discussed above.

Asymmetrically doped source and drain were commonly used for the suppression of ambipolar current in a TFET structure [20]. Lowered-doping concentration of drain enlarged the tunnel barrier width and reduced electric field at channel–drain heterointerface. The tunneling probability decreased exponentially with increasing tunnel barrier width. The I_{ON} depends on the BTBT current at the source–drain heterointerface, so it was less important to change in drain-doping concentration. Fig. 7 shows the drain current with two different drain-doping concentrations (10^{19} and 10^{18} cm^{-3}) with 2% strain in a p-type H-TFET. One can find that the I_{OFF} reduced as the doping concentration decreased, and meanwhile, the I_{ON} still remains the same, which is agreement with the mechanism described here.

D. Performance Evaluation With Different Strains

Fig. 8 shows I_{ON} as a function of increasing biaxial tensile strain for the n-type and p-type TFETs. Both homojunction

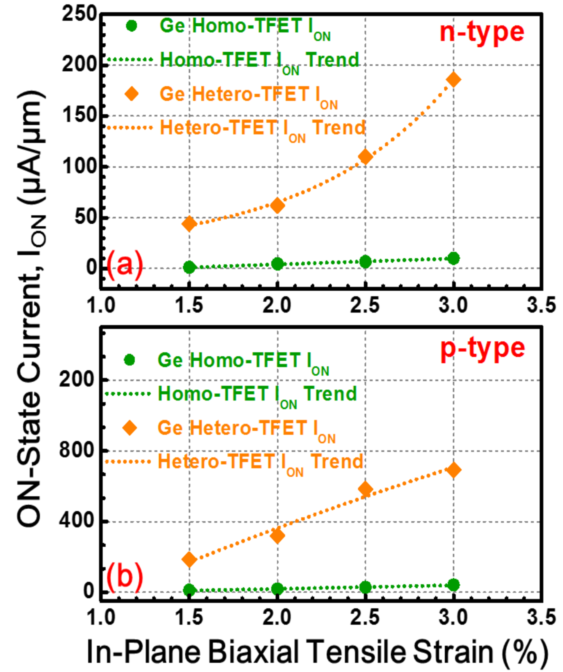

Fig. 8. Strain-induced enhancement of ON-state current for n-type and p-type homojunction (ε-Ge) and heterojunction (ε-Ge/$\text{In}_x\text{Ga}_{1-x}\text{As}$) TFETs.

TABLE II
BENCHMARKING

Reference	Type (Source/Channel)	V_{gs},V_{ds} (V)	I_{off} (μA/μm)	I_{on} (μA/μm)	SS (mV/dec)
Simulations					
Luisier, et al. IEDM,2009 [21]	n-type GaSb/InAs	0.5, 0.5	2.45E-5	752	~10.6
Sharma, et al. EDL,2014 [22]	n-type GaSb/InAs	0.5, 0.5	3E-3	235	~30
Liu, et al. ACS AMI, 2015 [23]	n-type GaAsSb/InGaAs	0.5, 0.5	6.20E-5	378	~11
This work	p-type InGaAs/ε-Ge (3%)	0.5, 0.5	1.01E-3	692	10
This work	n-type ε-Ge (3%)/InGaAs	0.5,0.5	1.33E-6	186	10
Experiments					
Zhou, et al. IEDM, 2012 [24]	p-type GaSb/InAs	0.5, 0.5	3E-2	180	200
Zhu, et al. JAP,2012 [25]	$\text{GaAs}_{0.35}\text{Sb}_{0.65}/\text{In}_{0.7}\text{Ga}_{0.3}\text{As}$	2.0, 0.5	1.21E-3	201	254
Bijesh, et al. IEDM, 2013[26]	$\text{GaAs}_{0.18}\text{Sb}_{0.82}/\text{In}_{0.6}\text{Ga}_{0.1}\text{As}$	0.5, 0.5	~2	176	>500

and heterojunction ε-Ge-based TFET architectures benefited from enhanced strain, however, H-TFETs have a significant reduction of effective barrier by staggered gap alignment. Consequently, the n-type H-TFETs showed a stronger dependence of I_{ON} on strain, as shown in Fig. 8, revealing an 18.6× increase in I_{ON} for the n-type H-TFETs at 3% tensile strain, whereas similarly strained p-type H-TFETs observed a 16.9× increase in I_{ON}. Furthermore, the simulated n- and p-type Ge/InGaAs H-TFETs have been benchmarked with reported experimental results for alternative high I_{ON} TFET device structures, as shown in Table II. One can find

This article has been accepted for inclusion in a future issue of this journal. Content is final as presented, with the exception of pagination.

from Table II that the reported Ge/InGaAs H-TFETs exhibit superior SS and high I_{ON} at low operating voltages (0.5 V).

IV. Conclusion

In summary, we have evaluated the band structure, the SS characteristics, the modulation of the effective tunneling barrier height, and the electrical performance of ε-Ge/In$_x$Ga$_{1-x}$As n- and p-type H-TFETs for the first time using numerical device simulation. The n-type H-TFETs demonstrated a substantial reduction in leakage current due to the higher tunneling barrier at the channel–drain interface. Both n- and p-type H-TFETs exhibited a significant enhancement in I_{ON} (18.6$\times$ and 16.9$\times$, respectively, at 3% strain) and which was attributed to both increased in strain and band discontinuities at the ε-Ge/In$_x$Ga$_{1-x}$As source–channel heterointerface. Furthermore, the p-type H-TFETs also benefited from a reduced conduction band offset as a result of doping-induced BGN, and thereby further reducing $E_{b_{\text{eff}}}$. In addition, point and average SS was reduced for both H-TFETs as compared with ε-Ge homo-TFETs. Therefore, the Ge-based H-TFETs show a great promise for low-power complementary TFET logic due to their ability to leverage improved channel carrier mobilities and a tunable $E_{b_{\text{eff}}}$. Furthermore, recently demonstrated composition modulation and strain engineering in Ge/In$_x$Ga$_{1-x}$As [8] provides a step toward achieving high drive current and low leakage Ge/InGaAs TFET devices presented here.

References

[1] Y. Zhu and M. K. Hudait, "Low-power tunnel field effect transistors using mixed As and Sb based heterostructures," *Nanotechnol. Rev.*, vol. 2, no. 6, pp. 637–678, Jun. 2013.

[2] J. Knoch and J. Appenzeller, "Modeling of high-performance p-type III–V heterojunction tunnel FETs," *IEEE Electron Device Lett.*, vol. 31, no. 4, pp. 305–307, Apr. 2010.

[3] R. Kotlyar *et al.*, "Bandgap engineering of group IV materials for complementary n and p tunneling field effect transistors," *Appl. Phys. Lett.*, vol. 102, no. 11, pp. 113106-1–113106-4, Mar. 2013.

[4] K.-H. Kao, A. S. Verhulst, W. G. Vandenberghe, B. Soree, G. Groeseneken, and K. de Meyer, "Direct and indirect band-to-band tunneling in germanium-based TFETs," *IEEE Trans. Electron Devices*, vol. 59, no. 2, pp. 292–301, Feb. 2012.

[5] S. Wirths *et al.*, "Band engineering and growth of tensile strained Ge/(Si)GeSn heterostructures for tunnel field effect transistors," *Appl. Phys. Lett.*, vol. 102, no. 19, pp. 192103-1–192103-4, 2013.

[6] S. Cho, I. M. Kang, T. I. Kamins, B.-G. Park, and J. S. Harris, Jr., "Silicon-compatible compound semiconductor tunneling field-effect transistor for high performance and low standby power operation," *Appl. Phys. Lett.*, vol. 99, no. 24, pp. 243505-1–243505-4, Dec. 2011.

[7] P. Guo *et al.*, "Tunneling field-effect transistor with Ge/In$_{0.53}$Ga$_{0.47}$As heterostructure as tunneling junction," *J. Appl. Phys.*, vol. 113, no. 9, pp. 094502-1–094502-9, Mar. 2013.

[8] M. Clavel, P. Goley, N. Jain, Y. Zhu, and M. K. Hudait, "Strain-engineered biaxial tensile epitaxial germanium for high-performance Ge/InGaAs tunnel field-effect transistors," *IEEE J. Electron Devices Soc.*, vol. 3, no. 3, pp. 184–193, May 2015.

[9] D. Rideau *et al.*, "Strained Si, Ge, and Si$_{1-x}$Ge$_x$ alloys modeled with a first-principles-optimized full-zone $k \cdot p$ method," *Phys. Rev. B*, vol. 74, no. 19, pp. 195208-1–195208-20, Nov. 2006.

[10] M. V. Fischetti and S. E. Laux, "Band structure, deformation potentials, and carrier mobility in strained Si, Ge, and SiGe alloys," *J. Appl. Phys.*, vol. 80, no. 4, pp. 2234–2252, Aug. 1996.

[11] V. Swaminathan and A. T. Macrander, *Materials Aspects of GaAs and InP Based Structures*. Upper Saddle River, NJ, USA: Prentice-Hall, 1991.

[12] A. Trellakis *et al.*, "The 3D nanometer device project nextnano: Concepts, methods, results," *J. Comput. Electron.*, vol. 5, no. 4, pp. 285–289, Dec. 2006. [Online]. Available: http://www.nextnano.de

[13] K.-H. Kao *et al.*, "Tensile strained Ge tunnel field-effect transistors: k·p material modeling and numerical device simulation," *J. Appl. Phys.*, vol. 115, no. 4, pp. 044505-1–044505-8, Jan. 2014.

[14] E. O. Kane, "Theory of tunneling," *J. Appl. Phys.*, vol. 32, no. 1, pp. 83–91, Jan. 1961.

[15] W.-S. Cho *et al.*, "Full band atomistic modeling of homo-junction InGaAs band-to-band tunneling diodes including band gap narrowing," *Appl. Phys. Lett.*, vol. 100, no. 6, pp. 063504-1–063504-3, Feb. 2012.

[16] R. Camacho-Aguilera, Z. Han, Y. Cai, L. C. Kimerling, and J. Michel, "Direct band gap narrowing in highly doped Ge," *Appl. Phys. Lett.*, vol. 102, no. 15, pp. 152106-1–152106-3, Apr. 2013.

[17] *TCAD Sentaurus User Guide*, Synopsys Inc., Mountain View, CA, USA, Ver. H-2013.03-sql., 2013.

[18] D. Chattopadhyay, S. K. Sutradhar, and B. R. Nag, "Electron transport in direct-gap III–V ternary alloys," *J. Phys. C, Solid State Phys.*, vol. 14, no. 6, pp. 891–908, Feb. 1981.

[19] M. El Kurdi, G. Fishman, S. Sauvage, and P. Boucaud, "Band structure and optical gain of tensile-strained germanium based on a 30 band $k \cdot p$ formalism," *J. Appl. Phys.*, vol. 107, no. 1, pp. 013710-1–013710-7, Jan. 2010.

[20] M. Schmidt *et al.*, "Unipolar behavior of asymmetrically doped strained Si$_{0.5}$Ge$_{0.5}$ tunneling field-effect transistors," *Appl. Phys. Lett.*, vol. 101, no. 12, pp. 123501-1–123501-4, Sep. 2014.

[21] M. Luisier and G. Klimeck, "Performance comparisons of tunneling field-effect transistors made of InSb, carbon, and GaSb-InAs broken gap heterostructures," in *IEDM Tech. Dig.*, Dec. 2009, pp. 37.6.1–37.6.4.

[22] A. Sharma, A. A. Goud, and K. Roy, "GaSb-InAs n-TFET with doped source underlap exhibiting low subthreshold swing at sub-10-nm gate-lengths," *IEEE Electron Device Lett.*, vol. 35, no. 12, pp. 1221–1223, Dec. 2014.

[23] J.-S. Liu, Y. Zhu, P. S. Goley, and M. K. Hudait, "Heterointerface engineering of broken-gap InAs/GaSb multilayer structures," *ACS Appl. Mater. Interf.*, vol. 7, no. 4, pp. 2512–2517, Jan. 2015.

[24] G. Zhou *et al.*, "Novel gate-recessed vertical InAs/GaSb TFETs with record high I_{ON} of 180 μA/μm at $V_{DS} = 0.5$ V," in *IEDM Tech. Dig.*, Dec. 2012, pp. 32.6.1–32.6.4.

[25] Y. Zhu *et al.*, "Defect assistant band alignment transition from staggered to broken gap in mixed As/Sb tunnel field effect transistor heterostructure," *J. Appl. Phys.*, vol. 112, no. 9, pp. 094312-1–094312-9, Nov. 2012.

[26] R. Bijesh *et al.*, "Demonstration of In$_{0.9}$Ga$_{0.1}$As/GaAs$_{0.18}$Sb$_{0.82}$ near broken-gap tunnel FET with $I_{ON} = 740$ μA/μm, GM $= 70$ μS/μm and gigahertz switching performance at $V_{DS} = 0.5$ V," in *IEDM Tech. Dig.*, Dec. 2013, pp. 28.2.1–28.2.4.

Jheng-Sin Liu (S'15) received the B.S. degree in electrical engineering from National Tsing Hua University, Hsinchu, Taiwan, in 2011, and the M.S. degree from the Graduate Institute of Photonics and Optoelectronics, National Taiwan University, Taipei, Taiwan, in 2013. He is currently pursuing the Ph.D. degree with the Bradley Department of Electrical and Computer Engineering, Virginia Polytechnic Institute and State University, Blacksburg, VA, USA.

Michael B. Clavel (S'09) received the B.S. degree in electrical engineering from the Virginia Polytechnic Institute and State University, Blacksburg, VA, USA, in 2013, where he is currently pursuing the Ph.D. degree with the Bradley Department of Electrical and Computer Engineering.

Mantu K. Hudait (M'08–SM'08) received the M.S. degree in materials science and engineering from IIT Kharagpur, Kharagpur, India, and the Ph.D. degree in materials science and engineering from the Indian Institute of Science, Bangalore, India, in 1999.

He joined the Bradley Department of Electrical and Computer Engineering, Virginia Polytechnic Institute and State University, Blacksburg, VA, USA, in 2009, as an Associate Professor.